Catalysis Today 181 (2012) 20–25

Contents lists available at SciVerse ScienceDirect

Catalysis Today

journal homepage: www.elsevier.com/locate/cattod

Evidence for an active oxygen species on Au/TiO_2(1 1 0) model catalysts during investigation with *in situ* X-ray photoelectron spectroscopy

K. Dumbuya[a], G. Cabailh[b], R. Lazzari[b], J. Jupille[b], L. Ringel[a], M. Pistor[a], O. Lytken[a], H.-P. Steinrück[a], J.M. Gottfried[a,c,*]

[a] *Lehrstuhl für Physikalische Chemie II, Universität Erlangen-Nürnberg, Egerlandstraße 3, 91058 Erlangen, Germany*
[b] *Institut de Nanosciences de Paris, Université Pierre et Marie Curie and CNRS, 4 Place Jussieu, 75005 Paris, France*
[c] *Philipps-Universität Marburg, Fachbereich Chemie, Hans-Meerwein-Straße, D-35032 Marburg, Germany*

ARTICLE INFO

Article history:
Received 21 March 2011
Received in revised form 18 August 2011
Accepted 21 September 2011
Available online 21 October 2011

Dedicated to Prof. Dr. Frigyes Solymosi on the occasion of his 80th birthday.

Keywords:
Catalysis
In situ photoelectron spectroscopy
Gold
Titania
Carbon monoxide
Oxygen
Oxidation

ABSTRACT

The influence of oxygen (O_2) and carbon monoxide (CO) on Au nanoparticles supported on TiO_2(1 1 0) in the size range of 2–3 nm has been studied using X-ray photoelectron spectroscopy (XPS) and *in situ* (high pressure) XPS at 300 K for O_2 and/or CO pressures of 0.1–1 mbar. These experiments were aimed at revisiting Au 4f core level shifts as reported in the literature and most importantly, to establish the dependence of the core-level shifts on the knowledge that there exists a maximum in reactivity for CO oxidation. Two samples were prepared with a coverage corresponding to that maximum (Au coverage 0.14–0.2 ML, particle size estimated to ~2–2.5 nm) while a third sample was expected to be less reactive (Au coverage 0.4 ML, particle size estimated to ~3.3 nm). At elevated O_2 pressures, a new Au 4f component at higher binding energy (2.4–2.6 eV relative to the Au(0) bulk signal) evolved at all particle sizes. Its appearance was attributed to a radiation-induced activation of oxygen and simultaneous oxidation of gold. The activation was much more efficient on the ~2–2.5 nm particles. The relative intensity of the oxide component depended strongly on O_2 pressure and, thus, on the equilibrium coverage of O_2. While not present in 0.1 mbar O_2 regardless of exposure time and particle size, it dominated the Au 4f spectrum of particles ~2–2.5 nm in size at 1 mbar oxygen pressure. This pressure-dependent formation reconciles previously conflicting XPS data. Finally, the activated oxygen species were very reactive toward CO as manifested by the rapid disappearance of the new Au 4f component in a 1:1 mixture of CO and O_2. The rates of evolution and consumption of this component were found to depend on gold coverage (and thus, particle size) and were highest for the smaller particles.

1. Introduction

Since its discovery, the origin of the catalytic activity of oxide-supported gold particles has been a matter of vivid controversy. Many efforts have been devoted to an understanding of the mechanistic aspects behind the unusually high catalytic activity of gold, in particular regarding the prototypical oxidation of carbon monoxide (CO). The interest in the CO oxidation reaction stems from potential practical applications in, for example, the purification of H_2 streams by selective oxidation of CO in order to avoid deactivation of Pt fuel cells. Since early reports by Haruta et al. [1], who showed the direct dependence of the catalytic activity on the Au cluster size, a series of models have been put forward, all in an effort to disentangle the mechanistic pathway of CO oxidation on Au. Today, there is a general consensus that the catalytic activity decreases drastically for particle sizes above 5 nm [2,3]. It is also nowadays a widely accepted view that the support material plays a significant role in the process by influencing the morphology and electronic configuration of the Au particles [4–7] although some groups advocate a lesser role of the support [8].

Numerous experimental methods have been applied in the search for the active site in the CO oxidation over supported gold catalysts. Photoelectron spectroscopy has been widely used in this regard, mainly because changes in the electronic state of small metal clusters can be routinely monitored using this technique. Lately, *in situ* implementations of this method have gained momentum due to their potential to identify mechanistically important transient species during reaction conditions. By *in situ* photoemission spectroscopy (*in situ* XPS) on an Au/TiO_2 powder catalyst, Willneff et al. [9] observed Au 4f core level shifts of +0.3 eV and +0.9 eV, which they assigned to bulk-like metallic gold and to intermediate gold species, respectively. The former is close to the

* Corresponding author at: Philipps-Universität Marburg, Fachbereich Chemie Hans-Meerwein-Straße, D-35032 Marburg, Germany. Tel.: +49 6421 2822541; fax: +49 6421 2822542.
E-mail address: michael.gottfried@chemie.uni-marburg.de (J.M. Gottfried).

0920-5861/$ – see front matter © 2011 Elsevier B.V. All rights reserved.
doi:10.1016/j.cattod.2011.09.035

0.3–0.4 eV shift reported by Herranz et al. [10] when Au/TiO_2(1 1 0) was exposed to a CO/O_2 mixture. Under the same conditions but with Au nanoparticles on a silica support, the same authors have also described a +0.3 eV shift of the Au 4f level at 423 K, but no such shift was found at room temperature.

Jiang et al. reported a very different Au 4f core-level shift of 2.3 eV toward higher binding energies when Au particles or Au foil were exposed to 1 Torr O_2 during *in situ* XPS measurements [11]. These results were explained by photon and photoelectron induced dissociative chemisorption of oxygen, in agreement with previous observations [12]. Similar Au 4f shifts have been observed for Au particles on TiO_2 and SiO_2 oxidized by oxygen plasma. Related temperature-programmed desorption (TPD) measurements confirmed that these shifts are due to chemisorbed atomic oxygen and gold oxide [13–15]. Beyond the fact that the observations of Jiang et al. deviate from those of Willneff et al., the conflicting results also question the applicability of *in situ* XPS to analyze the catalytic reaction itself [9,11].

By a simultaneous study of the reactivity and the particle morphology (size and shape), it has recently been shown [16] that the rate of the catalytic oxidation of CO on Au/TiO_2(1 1 0) films passes through a maximum for particles of 2–2.5 nm in diameter. On the basis of these findings, we have investigated Au/TiO_2(1 1 0) samples with different Au particle sizes representative of highly as well as poorly active conditions by *in situ* XPS in the presence of O_2, CO and a mixture of both gases in the 0.1–1 mbar range. These experiments were aimed at revisiting Au 4f core-level shifts as reported in the literature and to establish the dependence of the core-level shifts on the previously determined reaction rates. To address this issue systematically, three different Au/TiO_2(1 1 0) model catalysts were prepared, with particles close to the optimum size (~2 nm in size), and larger than the optimum size (~3 nm). The Au 4f, O 1s and Ti 2p levels were systematically recorded. In our experiments, previously reported Au core level shifts were convincingly reproduced. In addition, we observe two separate Au 4f core level shifts during a single experiment, unlike previous reports [9–11], and show that the 0.9 eV shift, whose origin has been controversially discussed in the literature (Au(I) oxide [17,18] versus final state effects [19–23]) is most likely due to final state effects.

2. Experimental

The XPS apparatus used for photoelectron and *in situ* photoelectron investigations of the Au/TiO_2 system allows conventional ultrahigh-vacuum (UHV) experiments but also high-pressure XPS (with reactive gas background pressures of up to 1 mbar) [24]. The key feature of this equipment is the efficient combination of four differential pumping stages between the sample (electron emission) and analyzer (electron detection) stages. The analyzer is a modified Omicron EA-125 unit and the X-ray source is a modified dual anode source (Specs XR-50) whose vacuum environment is completely isolated from that of the analysis chamber with the help of a 3 μm thick Al foil and additional gasket seals. The photon flux was approximately 4×10^9 photons/(cm^2 s). Gas dosing is achieved via flooding the main chamber (background dosing) with the required gas or via two capillary tubes that are directed at the surface of the sample (beam dosing). The background dosing method was utilized in this work. The base pressure in this chamber is in the low 10^{-9} mbar regime. A detailed description of this system is available in the work of Pantförder et al. [24].

The sample, a TiO_2 single crystal (dimensions 12 mm × 10 mm × 1 mm) with a polished (1 1 0) surface was mounted on a transferable home-made sample holder system, with the aid of which temperatures up to 1200 K are attainable via resistive heating. The temperature was measured using a thermocouple pair (type K) glued to the side of the crystal with ceramic glue (Aremco Ultra-Temp 516). The sputter source is a filament-free plasma device (Tectra) that enables sample bombardment in both inert gas and reactive gas environments. All sample preparation and Au evaporation were performed in a separate preparation chamber with a base pressure of 3×10^{-10} mbar. This chamber was also fitted with LEED optics (Varian), which was used to confirm the presence of a well-ordered TiO_2(1 1 0) surface, and a quadrupole mass spectrometer (Pfeiffer Prisma) for monitoring background gas concentrations.

Prior to each deposition episode, the TiO_2(1 1 0) surface was prepared by cycles of bombardment with Ar^+ ions and annealing to 1090 K for 15 min in an oxygen environment (5×10^{-6} mbar) according to established preparation procedures [25–28]. Au nanoparticles used in this study were prepared via vapor deposition of gold onto the TiO_2(1 1 0) surface under UHV conditions. The evaporator was a home-built Knudsen cell based on a ceramic tube which was filled with Au wire (99.999%, Goodfellow). Tungsten wire (0.2 mm thick) was wound along the tube for resistive heating. The temperature of the cell was measured by a type K thermocouple. Gold coverages were checked by three independent approaches, namely quartz microbalance, analysis of the damping of the XPS signal, and absolute calibration of the Au 4f signal with respect to the Au 4f peak collected on a Au(1 1 1) crystal. Two model catalysts with gold coverages of 0.14 ML and 0.2 ML were prepared by deposition at room temperature in vacuum to reproduce the coverage at which the sharply peaked maximum in catalytic activity for CO oxidation was observed in Ref. [16]. (A monolayer (ML) of gold corresponds to one Au(1 1 1) atomic layer, and is equivalent to 0.235 nm as measured by a quartz crystal microbalance.) A third sample with a coverage of 0.4 ML is expected to correspond to about half the maximum reactivity [16]. The exact determination and discussion of particle sizes are beyond the scope of the present paper. However, average particle sizes can be associated to the gold coverage under study on the basis of the 5 series of data recorded by 5 different groups that are shown in Fig. 5 of Ref. [16]. The average sizes corresponding to the maximum in reactivity and half that maximum are 2.5 nm and 3.3 nm, respectively. Based on the assumption that the maximum in reactivity corresponds to particles of 2.5 nm in size, particles obtained by deposition of 0.14 ML Au are estimated to be of ~2–2.5 nm in size [16,29,30]. Average sizes estimated in that way are used in the following to clarify the presentation.

Photoemission spectra of the Au 4f, Ti 2p, O 1s, and C 1s regions were recorded using Al Kα radiation (1486.6 eV). The Ti $2p_{3/2}$ binding energy was found herein to lie between 458.8 and 459.2 eV and, on bare samples, Au $4f_{7/2}$ was recorded in the 83.85–84.25 eV energy range. These are typical values found in tabulated data. Notably, the variations observed herein in the binding energy of Ti 2p and Au 4f are similar to shifts due to time-dependent X-ray irradiation damages in the case of Au/TiO_2 films [31]. The binding energies (BE) of all Au 4f core levels were corrected herein by using the Ti $2p_{3/2}$ binding energy of 459.0 eV which was previously established for a TiO_2(1 1 0) single crystal with sufficient conductivity to prevent charging under similar experimental conditions (analyzer transmission function, sample position, anode type and power).

Note that the usage of Ti 2p as the reference level in XPS can potentially lead to artifacts when comparing the peak positions of *in situ* and *ex situ* (UHV) experiments. It is known that pressures around 0.1–1 mbar cause a partial or complete de-charging on the surface during the *in situ* XPS experiment due to conductivity of the partially ionized gas phase. This may lead to a situation where the surface is (almost) neutral while the (near-surface) bulk is charged due to photoionization. This problem should be more manifest for high photon energies resulting in large electron escape depths.

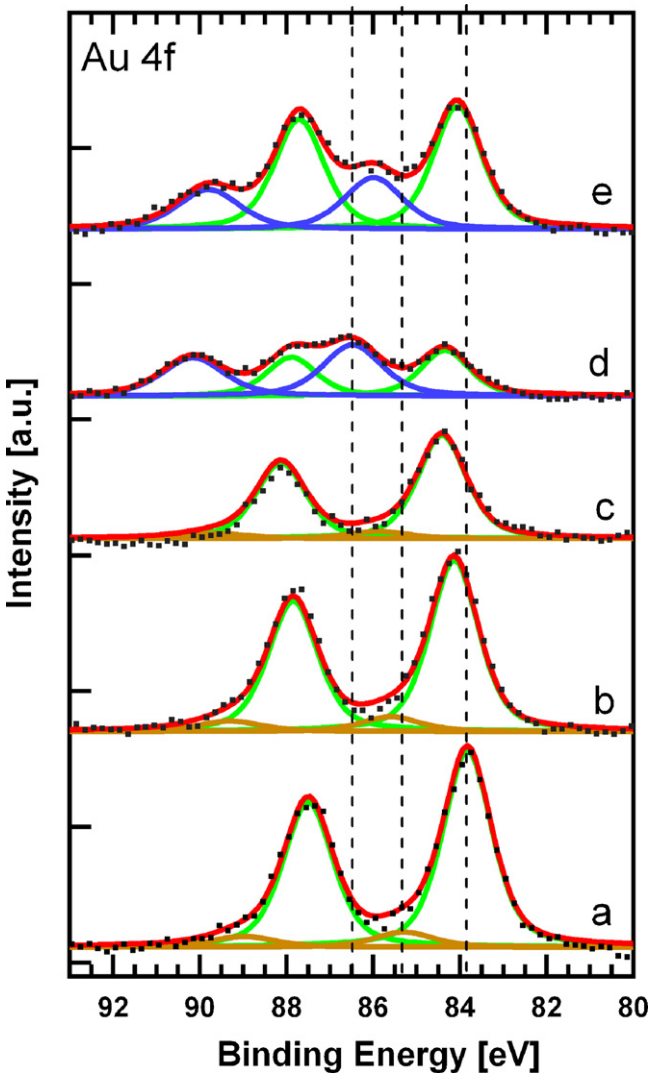

Fig. 1. *In situ* XP spectra of the Au 4f region of 0.4 ML Au (~3.3 nm Au clusters) on TiO_2(1 1 0). (a) As-prepared Au particles on TiO_2(1 1 0) at 300 K in UHV; (b) XPS in 0.1 mbar O_2, 1 h total exposure to X-rays; (c) XPS in 1 mbar O_2, 10 min exposure to X-rays; (d) XPS in 1 mbar O_2, 1 h exposure to X-rays; (e) UHV measurement following experiments in the presence of reactive gases.

The data acquisition times for the Au 4f spectra were 7.5 min for the high Au coverage (0.4 ML) and 15 min for the lower coverages. The Au 4f spectra were fitted using a combination of Gaussian and Lorentzian curves (pseudo Voigt function). Prior to peak deconvolution, a Shirley background was subtracted from all spectra. A $4f_{7/2}$ and $4f_{5/2}$ spin orbit splitting value of 3.65 eV and an area ratio of 4:3 were fixed for all fits.

3. Results and discussion

3.1. 0.4 ML Au on TiO_2(1 1 0): nanoparticles larger than the optimum size (~3.3 nm)

Fig. 1 shows Au 4f spectra for a sample with a Au coverage of 0.4 ML, which corresponds to Au nanoparticles with an average diameter estimated to ~3.3 nm, *i.e.* particles larger than the optimum size [16]. In Fig. 1a, the Au $4f_{7/2}$ peak maximum is centered at 83.9 eV. There is an additional minority species with a maximum at 85.2 eV, which has been observed previously (brown curves) [10]. The major Au $4f_{7/2}$ component can be assigned to metallic Au, while the nature of the minor component is controversial, as various authors have attributed this signal either to Au(I) [10,17,18] or to the finite size of the clusters combined with the insulating nature of the substrate, which results in a less efficient screening of the final core hole in the photoemission process [18–23], such that the positive Au 4f core-level shift induced by the final state charge outweighs the negative surface atom core-level shift [32]. This point will be further discussed in Section 3.3. When this sample was exposed to molecular oxygen (0.1 mbar, Fig. 1b) under X-rays for 1 h, the main peak shifted by 0.3 eV toward higher binding energy. The same shift was observed for Au/TiO_2 in a CO/O_2 mixture (partial pressures 0.1 Torr) at 423 K and attributed to electron density withdrawn from the Au particles by CO [10]. The finding of a similar shift in a pure O_2 atmosphere suggests that it is related to an oxygen equilibrium coverage rather than CO adsorption. At 0.1 mbar and regardless of exposure time, in agreement with the Willneff et al. [9], no other Au 4f component was observed.

During the first 10 min of oxygen exposure at 1 mbar (Fig. 1c), the main peak shifted further to higher binding energy by 0.2 eV relative to the peak at an O_2 pressure of 0.1 mbar and 0.5 eV relative to its UHV counterpart. The general intensity loss in 1 mbar O_2 is due to damping of the photoelectrons by the gas phase (compare Fig. 1a and c). About 40 min later under the same conditions, a strong new doublet whose signature dominated the entire spectrum had evolved at 86.5 eV and 90.2 eV, respectively (Fig. 1d, blue curves). With a shift close to that observed for Au_2O_3 [13–15,33], this doublet was assigned to chemisorbed oxygen and (at higher coverages) gold oxide. Atomic oxygen clearly results from the activation of molecular oxygen by X-ray photons and/or photoelectrons, as was hitherto suggested by Jiang et al. [11], since it does not show up without simultaneous exposure to X-rays. This observation is in line with previous studies on the activation of physisorbed O_2 on Au(1 1 0) by irradiation with UV photon or electrons, resulting in the formation of chemisorbed oxygen and gold oxide [34,35]. The subsequent XPS measurement under UHV conditions ($\sim 5 \times 10^{-8}$ mbar, Fig. 1e) revealed that the main Au 4f peak is still shifted toward higher binding energy by 0.3 eV with respect to the initial UHV measurement. A similar observation was made previously, following exposure of a reduced Au/TiO_2(1 1 0) sample to 20 mbar O_2 and subsequent XPS analysis in UHV (not shown). Moreover, the component at 86.5 eV is shifted by 0.7 eV toward lower binding energy following O_2 removal. This shift is most likely related to the formation of a non-stoichiometric, oxygen deficient Au-oxide species due to either reaction with background reductants such as CO (see Fig. 2) or to an X-ray induced decomposition of the oxide. The weight of this component decreases with respect to the overall Au 4f signal.

Peak widths used herein for the least-squares fits of the Au 4f spectra vary in a systematic way, mainly because of inhomogeneity broadening. The smallest full width at half maximum (fwhm) is found for the Au(0) peaks (green) of the pristine (not oxidized) samples. Peaks are narrower for the large particles (1.4 eV) than for the small clusters (1.7–1.9 eV). This is very reasonable, because the fraction of surface atoms (and other atoms with lower coordination numbers) and the fraction of Au atoms in contact with the TiO_2 substrate increase when the particles shrink. The Au(0) peak broadens by 0.1–0.2 eV when Au is oxidized, because now some of the Au(0) atoms are in contact to Au(III). Finally, the Au(III) peak is broader (>1.7 eV) than the Au(0) peak of the pristine sample, because it comprises a range of different species (Au with chemisorbed oxygen, gold oxides) with potentially slightly different binding energies. Those physically sound changes in width of components associated to only three different species were preferred to the alternative solution, which would have been to purposely add extra peaks. The assumption of the presence of only three gold species, together with the constraints for the spin-orbit splitting of the Au 4f signal, resulted in some cases in slight discrepancies between data

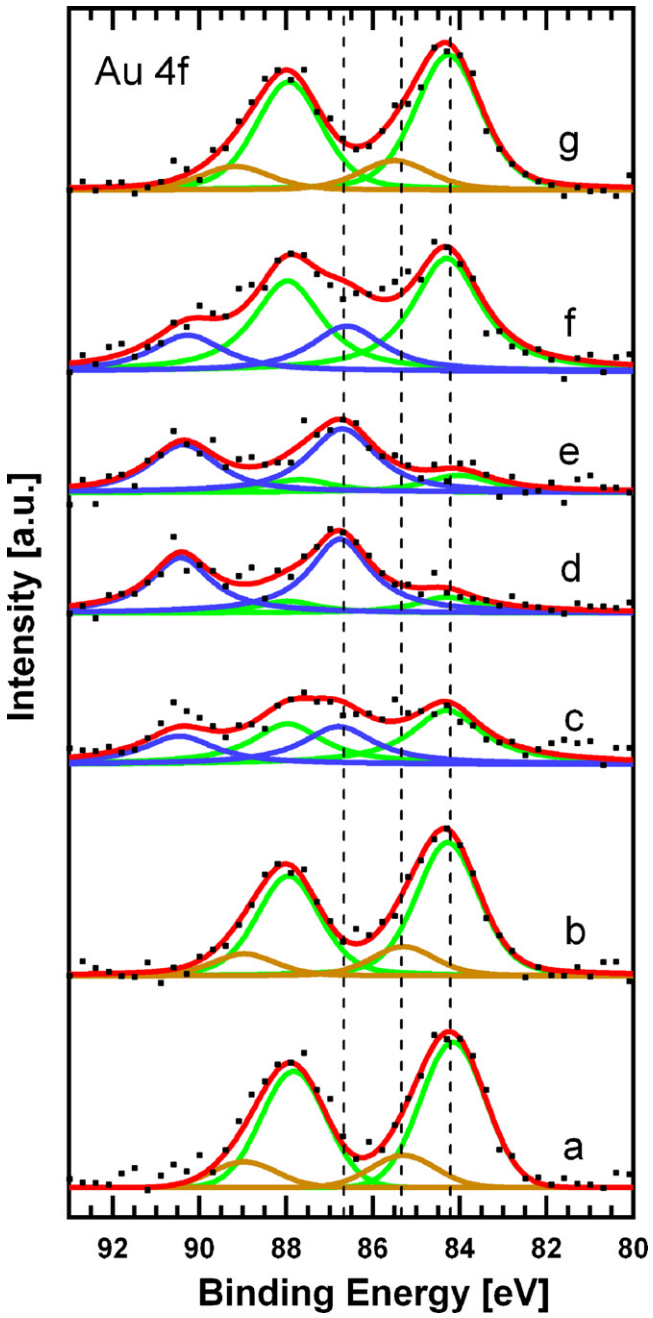

Fig. 2. *In situ* XP spectra of the Au 4f region of 0.2 ML Au (~2.5 nm Au clusters) on TiO_2(1 1 0). (a) As-prepared Au particles on TiO_2(1 1 0) at 300 K in UHV; (b) XPS in 0.1 mbar O_2, 1 h total exposure to X-rays; (c) XPS in 1 mbar O_2, 10 min exposure to X-rays; (d) XPS in 1 mbar O_2, 1 h exposure to X-rays; (e) after (d), but without X-rays for 30 min at 1 mbar O_2; (f) UHV XPS measurement after exposure to X-rays for 30 min in UHV; (g) UHV XPS measurement after 1 h in UHV.

points and fitted spectra. Statistical scatter of the data points also contributes to these deviations.

3.2. 0.2 ML Au on TiO_2(1 1 0): nanoparticles close to the optimum size (~2.5 nm)

In situ XPS data for particles in the size range with maximum CO oxidation activity (0.2 ML, size estimated to ~2.5 nm) are presented in Fig. 2. Spectra of bare clusters were similar to those observed in Fig. 1. The Au $4f_{7/2}$ peak appeared at a binding energy of 84.1 eV (green curves) and the additional Au $4f_{7/2}$ component (brown line at 85.3 eV) was again observed (see also Section 3.3 for a more detailed discussion of this component). The exposure to 0.1 mbar oxygen and X-rays caused no visible changes (Fig. 2b). However, in 1 mbar oxygen, Au oxide was rapidly formed (Fig. 2c) during the first 10 min of exposure, in stark contrast to the situation for larger particles (cf. Fig. 1c). After O_2 exposure at 1 mbar for 1 h (Fig. 2d), over 80% of the existing Au species were already in the oxidized state (blue curves), much more than in the case of the higher Au coverage (55% in the oxidized state, cf. Fig. 1d). These observations, in particular Fig. 2c, indicate that activation of molecular oxygen is more efficient than on the larger particles. Based on the widely accepted Langmuir–Hinshelwood mechanism for CO oxidation on Au, activation of dioxygen is considered to be a key step, followed by the consumption of atomic oxygen species by adsorbed CO to produce CO_2. In a true catalytic reaction, the activation of oxygen takes place spontaneously, whereas in our experiments, the process leading to chemisorbed oxygen and gold oxide is mainly radiation-induced. (Note that no accumulation of chemisorbed oxygen was observed in control experiments during which the sample was exposed to the same dosages of oxygen *without* simultaneous exposure to X-rays.) The rate of the radiation-induced formation of chemisorbed oxygen and gold oxide appears to be related to the particle size in a similar way as is the rate for the spontaneous CO oxidation. Possibly, both effects have a common origin. If the ~2.5 nm particles form the strongest bonds to O_2 molecules, this would explain the most efficient O_2 activation for the spontaneous CO oxidation, but also (due to the thus increased O_2 equilibrium coverage) the more efficient radiation-induced formation of chemisorbed oxygen or gold oxide.

It is noteworthy that the synchrotron experiments by Herranz et al. [10] and Jiang et al. [11] were run with a much higher photon flux ($\sim 4 \times 10^{14}$ photons cm^{-2} s^{-1}) than our experiment ($\sim 4 \times 10^{9}$ photons cm^{-2} s^{-1}). The X-ray exposure of 10 min reported in Ref. [11] corresponded to a total photon dose of 2.4×10^{17} photons/cm^2, whereas during 1 h our sample was only illuminated by 1.5×10^{13} photons/cm^2.

However, in both previous studies, the radiation-induced 2.4 eV Au 4f shift is not seen under a pressure of 0.1 mbar O_2 (compare Figs. 1b and 2b to data collected by Herranz et al. [10]) but observed under an oxygen pressure of 1 mbar (Figs. 1d and 2c to 2 g, and data of Jiang et al. [11]). The fact that five orders of magnitude in photon intensity do not change the conditions of pressure in which activation occurs indicates that the rate-limiting factor is the O_2 equilibrium coverage rather than the photon flux.

In addition, the absence of visible activation after 1 h of X-ray exposure under 0.1 mbar O_2 (Fig. 2b), while 10 min under 1 mbar O_2 lead to a 60% oxidation of gold, demonstrates that the activation rate does not depend linearly on the oxygen pressure. One reason for this is the consumption of chemisorbed oxygen (and gold oxide) by reaction with CO from the residual gas. If the rate of radiation-induced formation of chemisorbed oxygen (or gold oxide) is below the rate of its consumption, this oxygen species cannot accumulate. In addition, the presence of chemisorbed atomic oxygen on Au single crystal surfaces increases the desorption temperature of physisorbed dioxygen [12]. Therefore, chemisorbed oxygen should also increase the equilibrium coverage of dioxygen, which means that the radiation-induced formation of chemisorbed oxygen is a self-accelerated, autocatalytic and thus non-linear process. This, in combination with the constant removal of chemisorbed oxygen by residual CO explains the observation why no accumulation of chemisorbed oxygen is observed in 0.1 mbar O_2. Furthermore, it has been shown that dioxygen can dissociate on Au surfaces that are precovered with chemisorbed oxygen [36]. This mechanism could also contribute to an autocatalytic process, once an initial amount of chemisorbed oxygen is formed at a rate that is higher than the rate of consumption by reaction with residual CO. The consistency of the observations made in Berkeley [10,11], Berlin

[9] and in the present work increase the confidence about the pressure range (0.1 mbar–1.0 mbar) in which the oxygen coverage is high enough that the activation occurs.

Note that the adsorption energy of O_2 on low-indexed Au surfaces is very small at 12 kJ/mol for Au(1 1 0) [12]. Therefore, the O_2 equilibrium coverage is rather small on regular terrace sites, even at 1 mbar O_2 (below 10^{-4} ML, by extrapolation of the data in Ref. [12] to 300 K). However, oxygen adsorption is not only facilitated by pre-adsorbed atomic oxygen, as discussed above, it is also predicted to be facilitated by Au atoms with lower coordination numbers [37,38] and strain [37] which likely characterize supported gold nanoparticles such as those that catalyze the oxidation of CO. For example, Xu and Mavrikakis have found an adsorption energy of 25 kJ/mol for oxygen on stressed steps of Au(2 1 1) surfaces [37]. Assuming a desorption frequency prefactor of $10^{13\pm2}\,s^{-1}$ and a pressure of oxygen of 1 mbar, such energy leads to a coverage in the range of $\sim10^{+12\pm2}$ molecules/cm^2, the upper limit of which corresponds to a sizeable fraction of a monolayer.

Finally, it was found that the intensity of the 4f peak that corresponds to oxidized gold did not change when the X-ray source was shut down for 30 min (Fig. 2e). Since the intensity of the blue doublet decreases in vacuum conditions, either with (Fig. 2f) or without X-ray illumination (Fig. 2g), the observation is indicative of a continuous oxygen chemisorption under these conditions, because the intensity of this peak would have decreased due to reaction with background CO (cf. Fig. 2f and g). This is in agreement with previous reports by Deng et al. [36] who found that the dissociation probability of O_2 on Au(1 1 1) is increased by the presence of atomic oxygen on the surface. Exposure to X-ray photons in UHV removed atomic oxygen (Fig. 2f). However, in the absence of photons and O_2, the Au oxide is suggested to be rapidly reduced by background CO (cf. Figs. 1e and 2g), in agreement with previous observations on the reactivity of gold oxide toward CO [34,35] and with the results presented in the following section.

Because of the tight constraints applied in the least-square fit (see Section 3.1), statistical scatter of the data points leads to some small discrepancies between fit and data, visible for example for the peak around 90.5 eV in Fig. 2c. However, the presence of Au(III) in Fig. 2c is clearly evident from the presence of both spin-orbit components of the oxidized species.

3.3. *Au nanoparticles close to the optimum size under reactive conditions*

Particles used for this series of experiments were obtained by deposition of 0.14 ML Au and are estimated to be of ~2–2.5 nm in size (see Section 2). Having gained insight into the behaviour of the catalytically more active Au particles in oxygen in the 0.1–1 mbar regime, it was necessary to investigate these under CO oxidation conditions. The results are presented in Fig. 3. In the as-prepared sample, typical Au $4f_{7/2}$ binding energies of 84.0 eV and 84.8 eV are recorded. It is again observed that 0.1 mbar O_2 exposure does not cause gold oxide formation irrespective of particle size and duration of photon and oxygen exposure. The evolution of Au(III) was also observed in 0.5 mbar oxygen: after 1 h exposure, ~50% of the metallic gold was converted to the oxide (Fig. 3c).

The key message is that the activated oxygen reacts with CO, in agreement with the previously observed high reactivity of chemisorbed atomic oxygen and gold oxide that were produced by radiation-induced activation of oxygen toward CO [34,35]. When 0.5 mbar CO were introduced to the system already containing 0.5 mbar oxygen, the oxidic gold component was rapidly consumed while the signal of metallic gold evolved simultaneously (Fig. 3d). Experiments using the same gold coverage show that more than 50% of the oxidic component is consumed in the first 2 min of CO exposure.

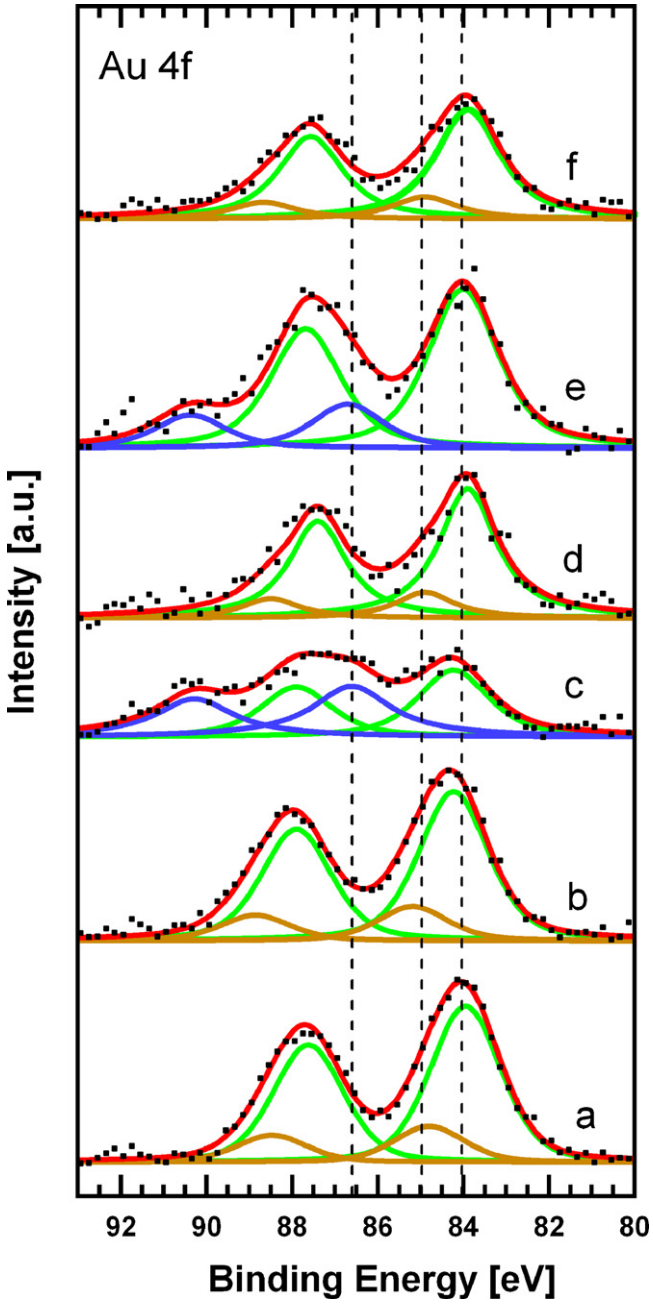

Fig. 3. *In situ* XP spectra of the Au 4f region of 0.14 ML Au (~2–2.5 nm Au clusters) on TiO_2(1 1 0). (a) As-prepared Au particles on TiO_2(1 1 0) at 300 K in UHV; (b) XPS in 0.1 mbar O_2, 1 h total exposure to X-rays; (c) XPS in 0.5 mbar O_2, 1 h exposure to X-rays; (d) XPS in a 1:1 mixture of CO + O_2, 1 mbar, 1 h total exposure to X-rays; (e) XPS in 0.5 mbar O_2 (CO off), 30 min exposure to X-rays; (f) UHV XPS measurement after 1 h in UHV (O_2 and CO off).

When shutting off CO while keeping the oxygen pressure to 0.5 mbar, the contribution of oxidic gold re-emerged (Fig. 3e). In the same way as in Section 3.2 (Fig. 2g), that component was completely consumed after 1 h in vacuum (Fig. 3f), most likely due to reaction with background CO. Exposure to X-ray photons in UHV might also contribute to the reduction of oxidized gold (Fig. 2f). As in Fig. 2, the small statistical discrepancies between fits and data in Fig. 3 do not question the deconvolution of the spectra into four components associated with Au(0) and Au(III).

Comparison of Figs. 1a, 2a and 3a reveals that the relative intensity of the component centered around 85 eV (brown curve) is smallest for the largest particles and almost identical for the two

samples with the smaller particles. Apparently, this component increases with decreasing Au coverage (and thus, decreasing cluster size). In Figs. 2g and 3f the component around 85 eV (brown curve) reappeared with its original intensity after 1 h in vacuum. The continued presence of this species under reducing UHV conditions, where the Au(III) oxide easily reacts with CO, supports the conclusion (see Section 3.1) that it is not Au in an oxidized state, such as Au(I) [10,17,18]. Instead, its origin may be traced back to poorly screened gold atoms [18–23,32], either due to the presence of very small clusters in the size distribution or due to gold atoms at the periphery of the (larger) clusters. Therefore, in Figs. 1b, 2b and 3b, the green and brown curves are assumed to be associated with metallic gold species.

4. Conclusions

Three Au/TiO_2(1 1 0) models catalysts were exposed to various partial pressures of oxygen (up to 1 mbar) and to a reactive CO + O_2 mixture, while being simultaneously analyzed by *in situ* photoelectron spectroscopy. Based on the knowledge that there is a reactivity maximum for CO oxidation, two samples were prepared with a coverage corresponding to that maximum (coverage 0.14–0.2 ML, particle size estimated to ~2–2.5 nm) while a third sample was expected to be less reactive (coverage 0.4 ML, particle size estimated to ~3.3 nm). The main observations can be summarized as follows:

(a) Deposition of gold onto TiO_2 leads to the appearance of the new Au 4f component, shifted by 0.9 eV to higher binding energy. This component, whose origin has been controversially discussed in the literature (Au(I) oxide [17,18] versus final state effects [19–23]), is most likely due to final state effects.
(b) Previously reported Au 4f core level shifts were convincingly reproduced herein. In addition, we observed two different Au 4f core level shifts during a single experiment, unlike previous reports [9–11]:
   - Upon exposure of large particles (~3 nm) to 0.1 mbar oxygen, the Au 4f core level shifts by 0.2–0.5 eV toward higher binding energy, which is attributed to charge transfer arising from oxygen adsorption either on the gold particles or at the interface between particles and substrate, but not from the formation of gold oxide;
   - Exposures to oxygen at pressures of 0.5–1.0 mbar lead to the appearance of a new Au 4f component shifted by 2.4 eV relative to the Au(0) signal. It is assigned to the radiation-induced formation of chemisorbed atomic oxygen that is a pivotal species in the study of surface chemistry of gold. This species, which leads to the formation of gold oxide, is not observed under 0.1 mbar O_2, but rapidly appears under 1 mbar O_2. This indicates that the rate of formation of this species depends on the O_2 equilibrium coverage. At low O_2 pressures (0.1 mbar), reaction with background CO prevents the accumulation of these reactive oxygen species. Finally, the activation of oxygen is size-dependent; it is much more efficient on the particles corresponding to the maximum in reactivity.
(c) Activated oxygen was found to be very reactive toward CO.

The origin and properties of the radiation-induced atomic oxygen is an important issue in the research focused on the understanding of catalysis by gold, because X-ray (and UV) photons are pivotal for studying structure [16] and chemistry [6,9–12,34,35] of supported gold. The way they induce surface reactions in the presence of gases must be carefully accounted for. In addition, the activation of oxygen is a method universally used to study the chemical properties of gold [12,34,35,39], so the cases under examination herein are representative of widely encountered conditions.

Acknowledgments

Financial support by the Deutsche Forschungsgemeinschaft through grant GO1812/1, by the Cluster of Excellence "Engineering of Advanced Materials", the French Agency for Research (Contract ANR07-NANO-024 REACTGOLD) and by the COST Action D41 "Inorganic Oxide Surfaces and Interfaces" is gratefully acknowledged.

References

[1] A. Ueda, T. Ohshima, M. Haruta, Appl. Catal. B: Environ. 12 (1997) 81.
[2] G.C. Bond, D.T. Thompson, Gold Bull. 37 (2000) 74.
[3] (a) R. Meyer, C. Lemire, S.K. Shaikhutdinov, H. Freund, Gold Bull. 37 (2004) 72; (b) M. Valden, X. Lai, D.W. Goodman, Science 281 (1998) 1647.
[4] A. Kolmakov, D.W. Goodman, Surf. Sci. Lett. 490 (2001) 597.
[5] B. Yoon, H. Häkkinen, U. Landman, A.S. Wörz, J.M. Antonietti, S. Abbet, K. Judai, U. Heinz, Science 307 (2005) 403.
[6] S. Arrii, F. Morfin, A.J. Renouprez, J.I. Rouset, J. Am. Chem. Soc. 126 (2004) 1199.
[7] R.J.H. Greisel, B.E. Nieuwenhuys, J. Catal. 199 (2001) 48.
[8] N. Lopez, T.V.W. Jansens, B.S. Clausen, Y. Xu, M. Mavrikakis, T. Bligaard, J.K. Norskov, J. Catal. 223 (2004) 232.
[9] E.A. Willneff, S. Braun, D. Rosenthal, H. Bluhm, M. Hävecker, E. Kleimenov, A. Knop-Gericke, R. Schlögl, S.L.M. Schroeder, J. Am. Chem. Soc. 128 (2006) 12052.
[10] T. Herranz, X. Deng, A. Cabot, P. Alivisatos, Z. Liu, G. Soler-Illia, M. Salmeron, Catal. Today 143 (2009) 158.
[11] P. Jiang, S. Porsgaard, F. Borondics, M. Köber, A. Caballero, H. Bluhm, F. Besenbacher, M. Salmeron, J. Am. Chem. Soc. 132 (2010) 2858.
[12] J.M. Gottfried, K.J. Schmidt, S.L.M. Schroeder, K. Christmann, Surf. Sci. 511 (2002) 65.
[13] L.K. Ono, B. Roldan Cuenya, J. Phys. Chem. C 112 (2008) 4676.
[14] J.M. Gottfried, J. Phys. Chem. C 112 (2008) 16721.
[15] L.K. Ono, B.R. Cuenya, J. Phys. Chem. C 112 (2008) 16723.
[16] I. Laoufi, M.-C. Saint-Lager, R. Lazzari, J. Jupille, O. Robach, S. Garaudée, G. Cabailh, P. Dolle, H. Cruguel, A. Bailly, J. Phys. Chem. C 115 (2011) 4673.
[17] J. Knecht, R. Fischer, H. Overhof, F. Hensel, J. Chem. Soc. Chem. Commun. 21 (1978) 905.
[18] Q. Fu, H. Saltsburg, M. Flytzani-Stephanopoulos, Science 301 (2003) 935.
[19] S. Lee, C.Y. Fan, T.P. Wu, S.L. Anderson, Surf. Sci. 578 (2005) 5.
[20] L. Oberli, R. Monot, H.J. Mathieu, D. Landolt, J. Buttet, Surf. Sci. 106 (1981) 301.
[21] T.T.P. Cheung, Surf. Sci. 140 (1984) 151.
[22] H.S. Shin, H.C. Choi, Y. Jung, S.B. Kim, H.J. Song, J. Shin, Chem. Phys. Lett. 383 (2004) 418.
[23] C.N.R. Rao, A.K. Santra, V. Vijayakrischnan, Top. Catal. 1 (1994) 25.
[24] J. Pantförder, J.F. Zhu, D. Borgmann, R. Denecke, H.-P. Steinrück, Rev. Sci. Instrum. 76 (2005) 014102.
[25] R.T. Zehr, M.A. Henderson, Surf. Sci. 602 (2008) 1507.
[26] M.B. Hugenschmidt, L. Gamble, C.T. Campbell, Surf. Sci. 302 (1994) 329.
[27] R.L. Kurz, R. Stockbauer, T.E. Madey, E. Roman, J.L. de Segovia, Surf. Sci. 218 (1989) 178.
[28] J.M. Pan, B.L. Manschoff, U. Diebold, T.E. Madey, J. Vac. Sci. Technol. A 10 (1992) 2470.
[29] X. Lai, T.P.St. Clair, M. Valden, D.W. Goodmann, Prog. Surf. Sci. 59 (1998) 25.
[30] M. Valden, S. Pak, X. Lai, D.W. Goodmann, Catal. Lett. 56 (1998) 7.
[31] N. Kruse, S. Chenakin, Appl. Catal. A: Gen. 391 (2011) 367.
[32] G.K. Wertheim, S.B. DiCenzo, S.E. Youngquist, Phys. Rev. Lett. 51 (1983) 2310.
[33] J.J. Pireaux, M. Liehr, P.A. Thiry, J.P. Delrue, R. Caudano, Surf. Sci. 141 (1984) 221.
[34] J.M. Gottfried, K.J. Schmidt, S.L.M. Schroeder, K. Christmann, Surf. Sci. 525 (2003) 184.
[35] J.M. Gottfried, K.J. Schmidt, S.L.M. Schroeder, K. Christmann, Surf. Sci. 525 (2003) 197.
[36] Y. Deng, B.K. Min, A. Guloy, C.M. Friend, J. Am. Chem. Soc. 127 (2005) 9267.
[37] Y. Xu, M. Mavrikakis, J. Phys. Chem. B 107 (2003) 9298.
[38] T.V.W. Janssens, B.S. Clausen, B. Hvolbæk, H. Falsig, C.H. Christensen, T. Bligaard, J.K. Nørskov, Top. Catal. 44 (2007) 15.
[39] T.A. Baker, X.Y. Liu, C.M. Friend, Phys. Chem. Chem. Phys. 13 (2011) 34.